

FULL PAPER

Copper(I) iodide supported on modified cellulose-based nano-magnetite composite as a biodegradable catalyst for the synthesis of 1,2,3-triazoles

Samaneh Sabaqian¹ | Firouzeh Nemati¹ | Majid M. Heravi² | Hossein Taherpour Nahzomi³

¹ Department of Chemistry, Semnan University, Semnan 35131-19111, Iran

² Department of Chemistry, School of Science, Alzahra University, Vanak, Tehran, Iran

³ Department of Chemistry, Payame Noor University, Tehran, Iran

Correspondence

Firouzeh Nemati, Department of Chemistry, Semnan University, Semnan 35131-19111, Iran.
Email: fnemati_1350@yahoo.com; fnemati@semnan.ac.ir

Nano-Fe₃O₄@Cellulose-NH₂-CuI as a novel magnetically separable composite was prepared and fully characterized using various techniques including Fourier transform infrared, X-ray photoelectron and energy-dispersive X-ray spectroscopies, X-ray diffraction, field-emission scanning and transmission electron microscopies, thermogravimetric analysis and vibrating sample magnetometry. To obtain an appropriate structure and also to describe to some extent the different kinds of metal–ligand interactions present in the nano-Fe₃O₄@Cellulose-NH₂-CuI composite, covalent and electrostatic interactions, density functional theory model chemistry and quantum theory of atoms in molecules method were employed, respectively. This cellulose-based heterogeneous catalyst can effectively promote the one-pot three-component reaction of a variety of terminal alkynes bearing substituted phenyls or propargylic alcohol together with substituted benzyl halides and sodium azide, so-called click reaction, in water to afford the corresponding 1,4-disubstituted 1,2,3-triazoles with improved yields and regioselectivity. The magnetic catalyst was conventionally recovered using an external magnet and reused in at least four successive runs under the optimal reaction conditions, without appreciable loss of its activity.

KEYWORDS

1,4-disubstituted 1,2,3-triazoles, biodegradable support, magnetic composite, metal–ligand interactions, quantum chemistry

1 | INTRODUCTION

Cellulose is the most abundant, inexpensive, renewable organic raw material on the earth. It is produced by nature at a rate of 10¹¹–10¹² tons per year.^[1–3] It is a carbohydrate polymer made up of repeating β-D-glucopyranose units and consists of three hydroxyl groups per anhydroglucose unit. In this way the cellulose molecule gains a high degree of functionality.^[4] The greater the OH functionality, the more the inter- or intramolecular hydrogen bonding, which is less attractive as a solid support.^[5] So, to get a higher degree of applicability and efficiency the surface needs to be modified.^[6] For this purpose, the introduction of amino groups onto the surface of cellulose via reaction with (3-aminopropyl)triethoxysilane (APTES) has been

successfully achieved and reported.^[7] The more nucleophilic amino group enhances the surface-modified cellulose performance especially as an electron donor ligand and a stronger metal–ligand interaction would be observed.^[8] All these features make it a good biocompatible support.^[3]

Catalysts play a key role in green chemistry by providing a clean and sustainable route for the organic synthesis of fine chemicals and intermediates.^[9] Nowadays, heterogeneous catalysis is attracting much attention. Conducting a reaction under heterogeneous catalysis shows several advantages such as ease of handling, toleration of a wide range of temperatures and pressures, and easy and inexpensive removal from reaction mixtures by filtration and centrifugation.^[10] Recently, biopolymers such as cellulose,^[11] chitosan^[12] or wool^[13] have been used in heterogeneous catalyst systems. Nevertheless,

their use as supports is restricted in industry due to their stable dispersion which hinders facile separation for recycling. For this reason, they have been coated with magnetic nanoparticles which leads to the formation of inorganic–organic hybrid nanocomposites.^[14] Magnetically recoverable catalysts often exhibit excellent selectivity, giving high yields, and have several additional advantages. They can be easily separated with purity, thus showing good reusability.^[15] Among them, magnetic iron oxide nanoparticles containing magnetite (Fe_3O_4) have been widely studied. They are highly efficient recoverable catalysts, and are useful in targeted drug delivery, clinical diagnosis, etc.^[16] In addition, they are nontoxic, mostly commercially available or easily accessible, amenable to functionalization and easy to handle.^[17]

Multicomponent coupling reactions are recognized as very powerful tools for the synthesis of various organic compounds from simple starting materials via a one-pot process. Especially, multicomponent reactions that provide polyfunctionalized heterocyclic compounds in a single operation are of great importance in synthetic organic and medicinal chemistry.^[18] Click chemistry is an important approach to the synthesis of drug-like molecules that can accelerate the drug delivery process by utilizing a few practical and reliable reactions, and has attracted much attention from biological and chemical points of view.^[19] ‘Click chemistry’ is a term that was introduced by Sharpless and co-workers in 2001 to describe reactions that exhibit high yields, high regio- and stereo-specificity and create only by-products that simply could be removed.^[20] During the last few decades, these types of reactions have attracted much attention in different fields of organic chemistry, material science and drug discovery.^[21] Huisgen 1,3-dipolar cycloaddition is the reaction of terminal alkynes, alkyl halides and sodium azide, providing 1,2,3-triazoles. Triazoles are an important class of heterocycles with a wide range of applications in various research fields. Examples are anti-HIV activity,^[22] antibacterial activity,^[23] anti-allergic activity,^[24] agrochemicals, dyes, corrosion inhibitors, photostabilizers and photographic materials.^[25] Triazoles are usually produced through copper-catalysed azide–alkyne cycloaddition,^[26] which is one of the most reliable click reactions,^[27] and has provided a practical and efficient route to prepare 1,4-disubstituted 1,2,3-triazoles, from a wide range of substrates with excellent selectivity.^[28] Unfortunately, the copper compounds usually lead to considerable amount of salt-containing effluent beside the desired products. They are not easy to handle, are difficult to separate and have limited reuse potential often due to contamination with final products or formation of metal complexes. So, immobilization of catalysts on suitable insoluble supports is one of the most reliable methods for improving the efficiency and recovery of catalysts and strongly recommended from the viewpoint of green chemistry.^[29] Zeolites,^[30] montmorillonite,^[31] polystyrene,^[32] chitosan^[33] and modified KIT-5^[34] are some of the notable supports that bring about the heterogeneous catalysis of regioselective,

three-component reactions of alkyl halides, sodium azide and terminal alkynes.

Enhanced environmental consciousness has promoted the efficiency of chemical reactions under benign conditions with recycling and reuse of catalysts, a trait that has become an adjunct of much chemical research today.^[35] In this regard, cellulose base materials could be attractive as potential supports in heterogeneous catalysis due to low cost, biodegradability, stability against various chemical environments and low toxicity.

In continuation of our studies of the design of nanomagnetic heterogeneous catalysts^[36] and their applications in several organic transformations^[37] and our efforts to develop regioselective synthesis of 1,4-disubstituted 1,2,3-triazoles via click reaction,^[38] in the present paper, we describe the preparation and characterization of a novel nano-magnetic cellulose-based CuI composite as a recoverable heterogeneous catalyst. The catalytic application of this magnetic composite was examined in the reaction of phenylacetylene, benzyl bromide and sodium azide in water as a model reaction, which proceeded smoothly to afford the corresponding 1,4-substituted 1,2,3-triazole as sole product, regioselectively.

2 | EXPERIMENTAL

2.1 | Materials and instrumentation

Chemical reagents of high purity were purchased from Merck and Aldrich and were used without further purification. Melting points were determined in open capillaries using an Electrothermal 9100 without further corrections. Fourier transform infrared (FT-IR) spectra were obtained with potassium bromide pellets in the range $400\text{--}4000\text{ cm}^{-1}$ using a Shimadzu 8400 s spectrometer. X-ray diffraction (XRD) was conducted with a Philips instrument using $\text{Cu K}\alpha$ radiation with a wavelength of 1.54 \AA . Field-emission scanning electron microscopy (SEM) in conjunction with energy-dispersive X-ray (EDX) analysis was performed using a Tescanvega II XMU digital scanning microscope. Samples were coated with gold at 10 mA for 2 min prior to analysis. The magnetic properties were characterized using vibrating sample magnetometry (VSM; Lakeshore7407) at room temperature. Transmission electron microscopy (TEM) was performed using a CM30 300 kV digital transmission microscope. X-ray photoelectron spectroscopy (XPS) was conducted using a Gamdata-scienta ESCA200 hemispherical analyser equipped with an $\text{Al K}\alpha$ (1486.6 eV) X-ray source.

2.2 | Preparation of catalyst

2.2.1 | Preparation of cellulose- NH_2

Reactive amino groups were introduced onto the surface of cellulose materials by reaction of cellulose with APTES. In brief, dried cellulose microcrystals (0.2 g) were mixed with

APTES (2.86 mmol) and anhydrous dimethylformamide (DMF; 20 ml). The reaction lasted for 2 h at room temperature. The activated cellulose substrates were separated by centrifugation, rinsed with anhydrous DMF three times and dried.^[7]

2.2.2 | Preparation of nano-Fe₃O₄@Cellulose-NH₂-CuI

Magnetic nanoparticles were obtained by alkaline hydrolysis of iron(II) chloride and iron(III) chloride (molar ratio of 1:2) in aqueous solution according to the co-precipitation method described in our earlier report.^[37] The magnetic composite was prepared by adding an aqueous solution of cellulose-NH₂ (2 wt%) to an aqueous mixture of the magnetic nanoparticles (10 mg ml⁻¹) and CuI (500 mg). The resulting mixture, CuI, cellulose-NH₂ and magnetic nanoparticles (nanoparticles-to-cellulose ratio of 1:1 v/v), was heated at 80 °C and magnetically stirred for 5 h under nitrogen atmosphere. The mixture was filtered magnetically and the obtained solid, nano-Fe₃O₄@Cellulose-NH₂-CuI, was washed with water and dried under vacuum at 60 °C.

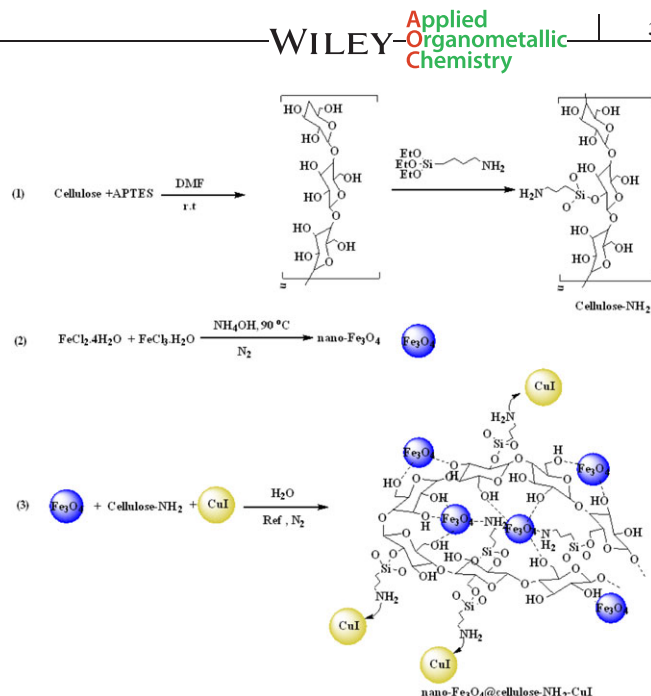
2.3 | Synthesis of 1-Benzyl-4-phenyl-1*H*-1,2,3-triazole: general procedure

Nano-Fe₃O₄@Cellulose-NH₂-CuI (0.01 g) was added to a solution of phenylacetylene (0.102 g, 1 mmol), benzyl chloride (0.126 g, 1 mmol) and NaN₃ (0.071 g, 1.1 mmol) in water (3 ml). The reaction mixture was magnetically stirred under reflux for the required time. The progress of the reaction was monitored by TLC (*n*-hexane–ethyl acetate, 7:3). Upon completion of the reaction, the solution was decanted. The leftover residue was diluted with hot ethanol and the catalyst was separated from this mixture using an external magnet, washed with acetone (2 × 10 ml), dried in an oven and stored for use in subsequent runs under the same conditions. After separation of catalyst, the solution was evaporated to dryness, and crude product was obtained. The residue was purified by recrystallization from EtOH–H₂O (3:1 v/v) to afford 1-benzyl-4-phenyl-1*H*-1,2,3-triazole (0.22 g, 95%). Some products had to be purified by chromatography on silica gel, using a short column.

3 | RESULTS AND DISCUSSION

3.1 | Catalyst preparation

Scheme 1 shows the synthesis of the nano-Fe₃O₄@Cellulose-NH₂-CuI magnetic composite. The nano-magnetic composite was prepared from commercially available, inexpensive materials. In the first step, cellulose was successfully functionalized using APTES in DMF at room temperature. The magnetic Fe₃O₄ nanoparticles were prepared by co-precipitation of iron(II) and iron(III) ions in alkali medium. Then, nano-Fe₃O₄@Cellulose-NH₂-CuI was prepared by adding an aqueous solution of cellulose-NH₂ (2 wt%) to an aqueous



SCHEME 1 Preparation of nano-Fe₃O₄@Cellulose-NH₂-CuI catalyst

mixture of the magnetic nanoparticles (10 mg ml⁻¹) and CuI (200 mg) (Scheme 1). The structural and chemical nature of the catalyst was characterized using the corresponding data provided by FT-IR spectroscopy, XRD, SEM, TEM, VSM, XPS and thermogravimetric analysis (TGA).

3.2 | Catalyst characterization

3.2.1 | FT-IR spectra

The FT-IR spectra of nano-Fe₃O₄, cellulose, cellulose-NH₂ and nano-Fe₃O₄@Cellulose-NH₂-CuI were recorded and are depicted in Figure 1. As can be seen in the spectrum of nano-Fe₃O₄ (Figure 1a), the strong band at 595 cm⁻¹ corresponds to Fe–O vibration, and the bands at 3420 and

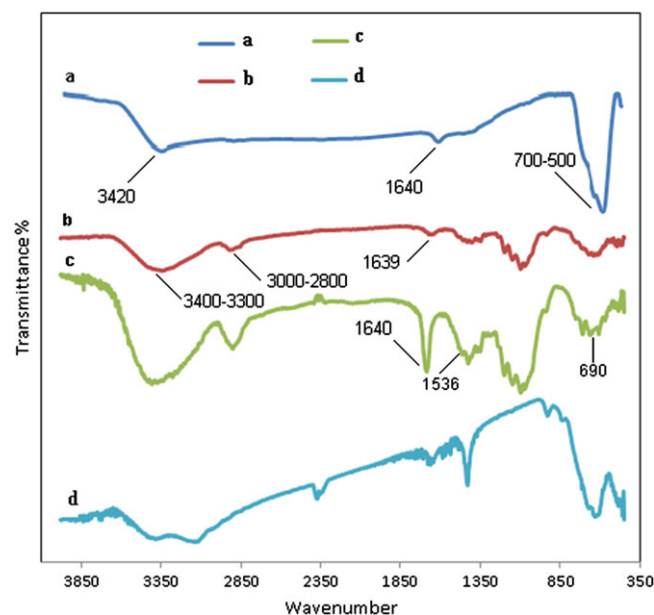


FIGURE 1 FT-IR spectra of (a) nano-Fe₃O₄, (b) cellulose, (c) Cellulose-NH₂ and (d) nano-Fe₃O₄@Cellulose-NH₂-CuI

1630 cm^{-1} are assigned to the stretching and bending vibrations of hydroxyl groups on the surface of Fe_3O_4 nanoparticles.^[39] Typical wavenumbers for hydroxyl groups for cellulose, such as $-\text{CH}-\text{OH}$ and $-\text{CH}_2-\text{OH}$ stretching, are in the range $3300\text{--}3400\text{ cm}^{-1}$. The methylene group stretching bands, from the incorporated molecule, are located at 2900 cm^{-1} and the band in the range $2800\text{--}3000\text{ cm}^{-1}$ is attributed to $-\text{C}-\text{H}$ groups. The bending vibrations of OH on the cellulose surface are located at 1639 cm^{-1} , the primary and secondary hydroxyl bending bands appear in the range $1200\text{--}1500\text{ cm}^{-1}$ and C–O stretching vibration is observed at 1100 cm^{-1} (Figure 1b).^[39,40] After functionalization of cellulose, the N–H bending vibration at around 690 cm^{-1} , NH_2 symmetric bending vibration at 1536 cm^{-1} and stretching vibration of C–N at 1220 cm^{-1} confirm the presence of APTES moieties on the cellulose surface^[4] (Figure 1c). A decrease in intensity of broad band due to hydroxyl groups (Figure 1d) indicates the interaction of modified cellulose with nano- Fe_3O_4 and CuI, which was further verified from other techniques.

3.2.2 | XRD analysis

Figure 2 shows XRD patterns of as-synthesized nano- Fe_3O_4 , cellulose, cellulose- NH_2 and nano- Fe_3O_4 @Cellulose- NH_2 -CuI. The typical diffraction peaks located approximately at 30.1° , 35.5° , 43.2° , 53.4° , 57.1° and 62.7° can be well assigned to the diffraction of Fe_3O_4 nanoparticles with cubic phase from the (111), (220), (311), (400), (422), (511) and (440) planes, respectively^[41] (Figure 2a).

It is clear that the cellulose and modified cellulose have typical diffraction angles at around 14.87° , 16.25° and 22.64° (Figure 2b and c).^[2] In the XRD pattern of nano- Fe_3O_4 @Cellulose- NH_2 -CuI (Figure 2d), the characteristic peaks of cellulose and Fe_3O_4 are observed, indicating that the Fe_3O_4 nanoparticles are embedded in the modified cellulose and the Fe_3O_4 structure had not changed. The mean

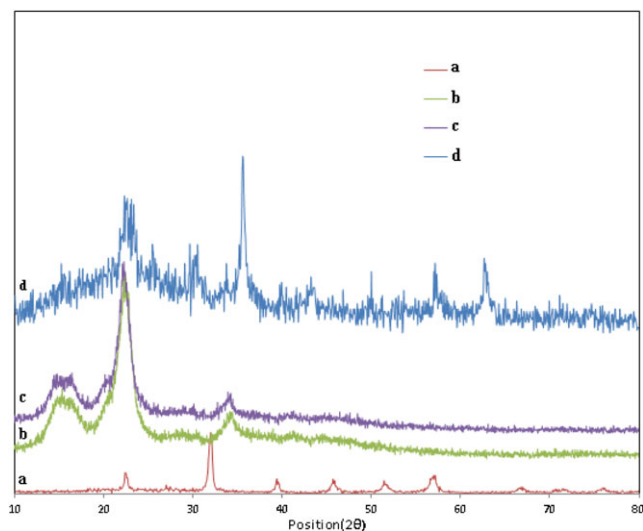


FIGURE 2 XRD patterns of as-synthesized (a) nano- Fe_3O_4 , (b) cellulose, (c) Cellulose- NH_2 and (d) nano- Fe_3O_4 @Cellulose- NH_2 -CuI

diameter of Fe_3O_4 crystallite was determined using Scherrer's equation to be 8.91 nm. The characteristic peaks at 2θ of 25.5° , 29.5° , 42.2° , 50.0° , 61.2° , 67.45° and 77.20° can be attributed to cubic CuI (JCPDS card no. 01-076-0207), which strongly evidences the immobilization of CuI on the nano-magnetic composite (Figure 2d). However, the amount of CuI particles is very low relative to carriers so that the diffraction peaks are very weak.

3.2.3 | SEM, EDX and TEM

The morphology and chemical purity of nano- Fe_3O_4 @Cellulose- NH_2 -CuI were investigated using SEM (Figure 3a) and EDX analysis (Figure 4a). Appearance of Au element in EDX analysis shows the material being coated by a layer of Au for by EDX and SEM characterization. Figure 3(a) shows the SEM image of nano-

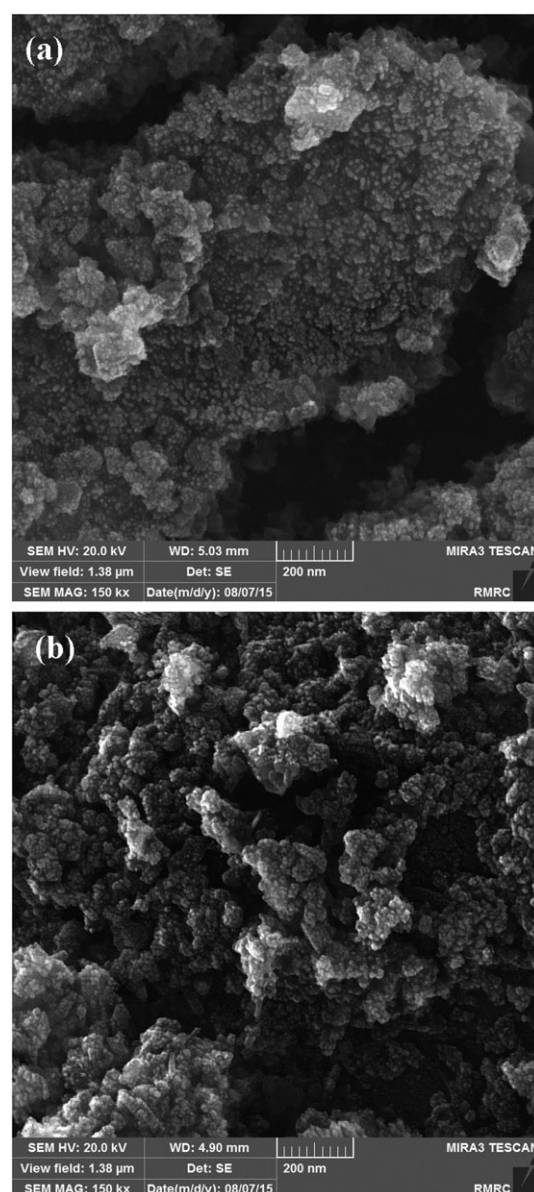


FIGURE 3 SEM images of surface of (a) nano- Fe_3O_4 @Cellulose- NH_2 -CuI and (b) nano- Fe_3O_4 @Cellulose- NH_2

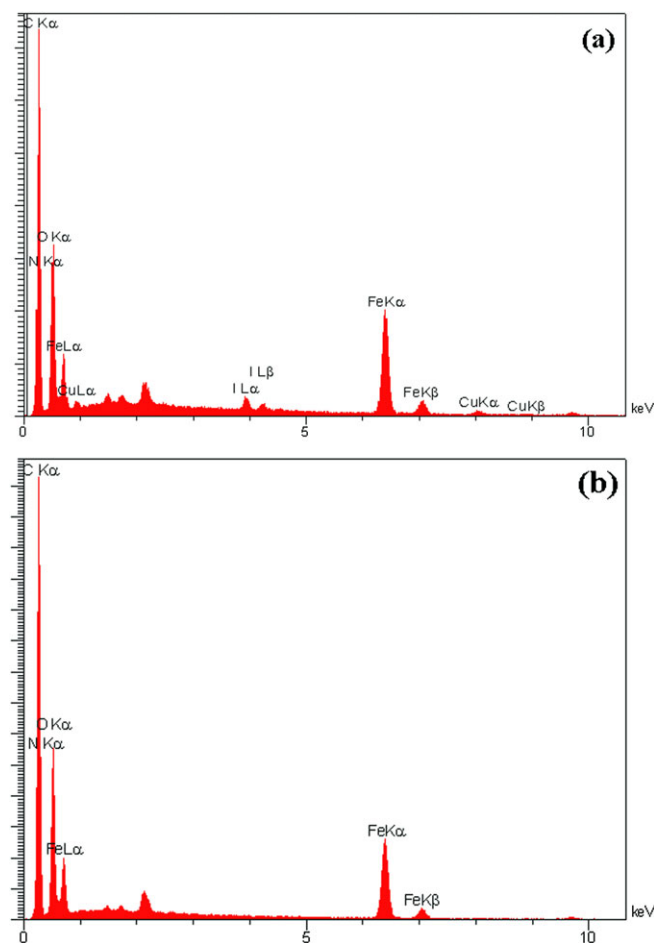


FIGURE 4 EDX spectra of surface of (a) nano-Fe₃O₄@Cellulose-NH₂-CuI and (b) nano-Fe₃O₄@Cellulose-NH₂

Fe₃O₄@Cellulose-NH₂-CuI with the optimized amount of CuI required for catalytic activity. The morphology of the composite displays a homogeneous structure. As shown in Figure 4(a), the EDX spectrum of nano-Fe₃O₄@Cellulose-NH₂-CuI indicates that there are C, O, N, Fe, Cu and I elements in the catalyst that confirms the presence of CuI along with iron in the structure of nano-Fe₃O₄@Cellulose-NH₂-CuI. The amount of CuI loading in nano-Fe₃O₄@Cellulose-NH₂ is estimated to be 2.25% from EDX analysis (Figure 4a). Also, for comparison, SEM image and EDX spectrum of nano-Fe₃O₄@Cellulose-NH₂ are shown in Figures 3(b) and 4(b). A comparison of Figure 3(a) and (b) with Figure 4(a) and (b) indicates that CuI is loaded on nano-Fe₃O₄@Cellulose-NH₂. This also guarantees the immobilization of CuI species on nano-Fe₃O₄@Cellulose-NH₂.

A TEM image of the prepared nano-Fe₃O₄@Cellulose-NH₂-CuI is shown in Figure 5. The TEM image shows the existence of three regions with different size and electron density which confirms the formation of the composite: two electron-dense regions of different sizes which correspond to Fe₃O₄ nanoparticles and CuI microparticles and a less dense and more translucent region which corresponds to cellulose matrix. Figure 5 confirms the stable and homogeneous dispersion of Fe₃O₄ nanoparticles on the surface of modified cellulose.

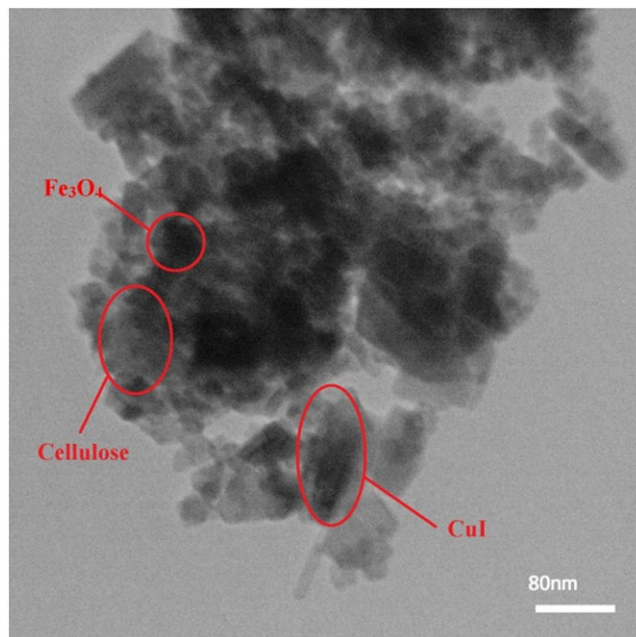


FIGURE 5 TEM image of nano-Fe₃O₄@Cellulose-NH₂-CuI

3.2.4 | Magnetization study

The magnetic behaviour of the as-synthesized nano-Fe₃O₄, nano-Fe₃O₄@Cellulose-NH₂ and nano-Fe₃O₄@Cellulose-NH₂-CuI was investigated using VSM. The magnetization curves were recorded at room temperature and are shown in Figure 6. The saturation magnetization of the uncoated nanoparticles is 61.6 emu g⁻¹, which is typical for maghemite nanoparticles. The nano-Fe₃O₄@Cellulose-NH₂ and nano-Fe₃O₄@Cellulose-NH₂-CuI samples have saturation magnetizations of 22.13 and 21.11 emu g⁻¹, respectively. Due to the nonmagnetic properties of amino-modified cellulose and CuI on the particle surface, the mean saturation magnetization decreases after the coating process. The difference

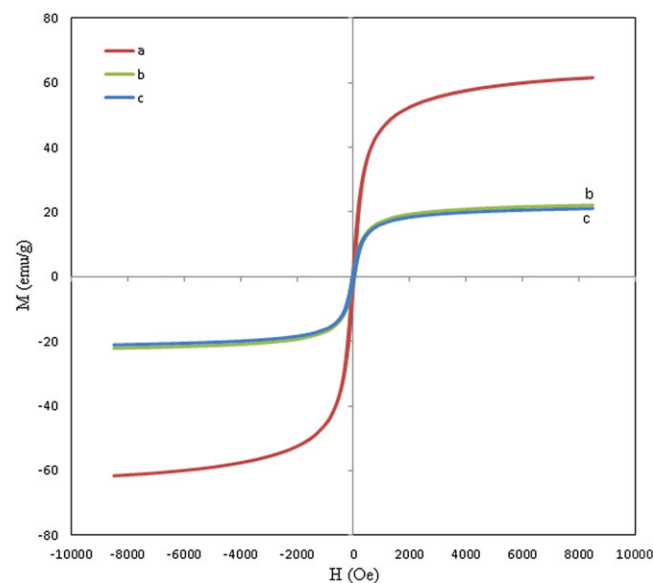


FIGURE 6 Magnetic hysteresis curves for as-synthesized (a) nano-Fe₃O₄, (b) nano-Fe₃O₄@Cellulose-NH₂ and (c) nano-Fe₃O₄@Cellulose-NH₂-CuI

between magnetic saturation of nano- Fe_3O_4 @Cellulose- NH_2 and nano- Fe_3O_4 @Cellulose- NH_2 -CuI is negligible. Clearly, with such high saturated magnetization, the nano- Fe_3O_4 @Cellulose- NH_2 -CuI could be easily and quickly separated from a reaction mixture by applying an external magnet field.

3.2.5 | XPS analysis

The XPS elemental survey scan of the surface of the nano- Fe_3O_4 @Cellulose- NH_2 -CuI composite is shown in Figure 7. Peaks corresponding to carbon, oxygen, iron, iodine and copper are clearly observed.

The corresponding high-resolution XPS spectra of C 1s, O 1s and Fe 2p regions are shown in Figure 8. The XPS spectra show two major peaks with binding energies of *ca* 293.82 and 539 eV, corresponding to C 1s (Figure 8a) and O 1s (Figure 8b), respectively, and characteristic of the presence of the cellulose phase.^[42] The peaks appearing in Figure 8c are located at 709.23 and 723.88 eV, which are ascribed to Fe 2p_{3/2} and Fe 2p_{1/2} of Fe in Fe_3O_4 .^[43] Because of the low loading of CuI in the nano- Fe_3O_4 @Cellulose- NH_2 -CuI composite, very faint signals appear at 942.3 and 962.5 eV. They are assigned to Cu^+ state, which is in accordance with the data reported in the literature.^[37]

3.2.6 | Thermogravimetric analysis

In order to obtain information on the thermal stability, TGA experiments were carried out by heating nano- Fe_3O_4 , cellulose, cellulose- NH_2 and nano- Fe_3O_4 @Cellulose- NH_2 -CuI up to 600 °C in air. These experiments confirm the functionalization of cellulose and the presence of Fe_3O_4 and CuI in the composite (Figure 9).

Figure 9(a) shows the TGA curve for bare Fe_3O_4 nanoparticles. The curve reveals little change in terms of mass loss. Loss of strongly adsorbed water and dehydration of surface hydroxyl groups occur at approximately 250 °C. Pure cellulose shows a 5–10% weight loss between 35 and

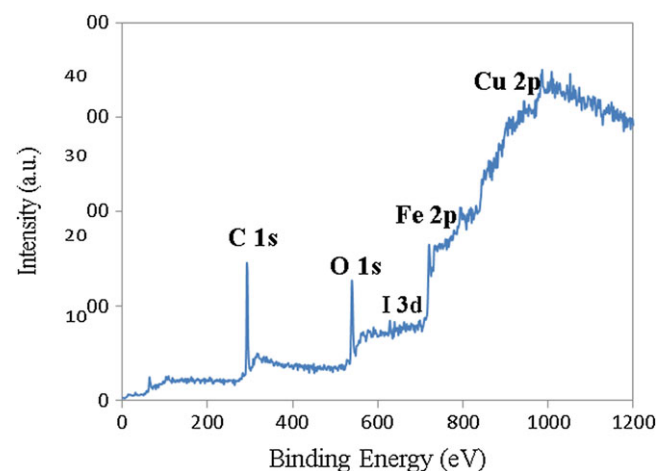


FIGURE 7 XPS pattern of as-synthesized nano- Fe_3O_4 @Cellulose- NH_2 -CuI composite

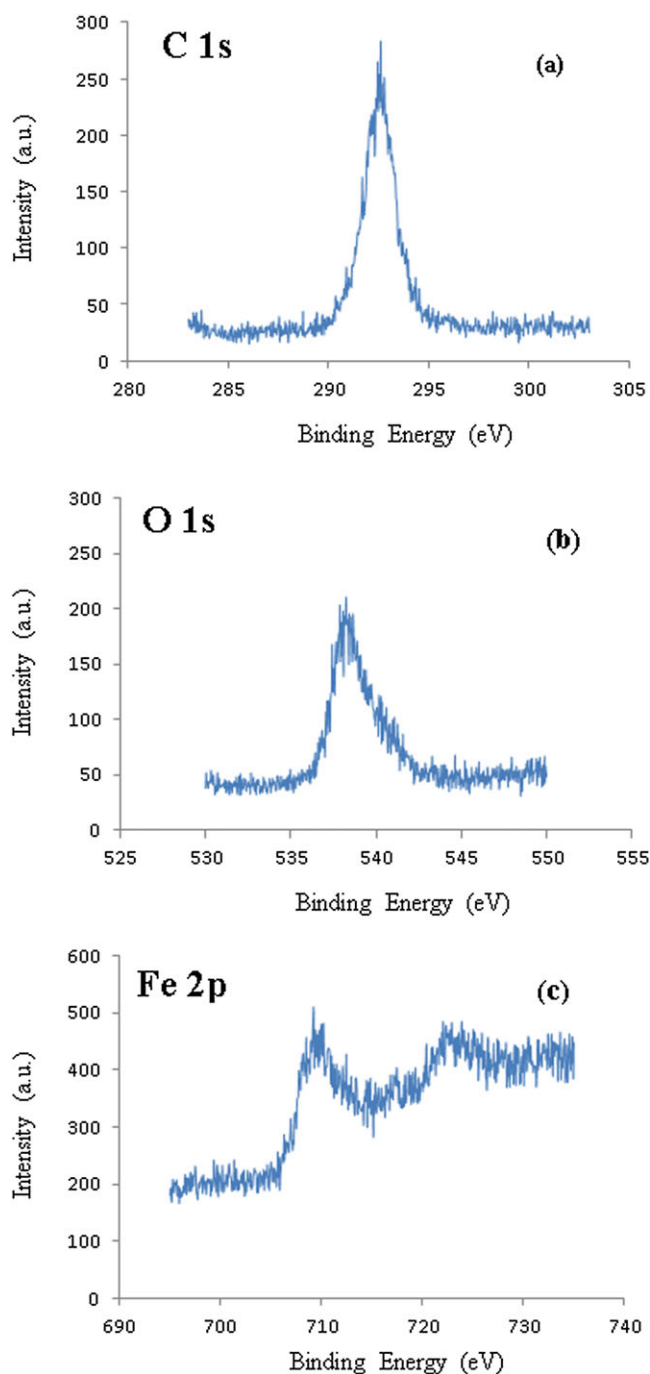


FIGURE 8 High-resolution XPS spectra of nano- Fe_3O_4 @Cellulose- NH_2 -CuI composite: (a) C 1s; (b) O 1s; (c) Fe 2p

150 °C, due to the evaporation of adsorbed moisture. Another sharp mass loss appears at 275 °C, which could be attributed to the degradation of cellulose chains.^[1] For cellulose- NH_2 the decomposition process can be divided into two stages within the range from 35 to 500 °C. Between 35 and 150 °C, the initial weight loss of the samples is below 5–10%, presumably due to the evaporation of adsorbed water. At higher temperatures (150–500 °C), a different pattern of loss of weight from cellulose can be seen, indicating the degradation of organic material, that is, aminocellulose.^[2] The weight loss of nano- Fe_3O_4 @Cellulose- NH_2 -CuI is about 60% at 270–320 °C, corresponding to the thermal

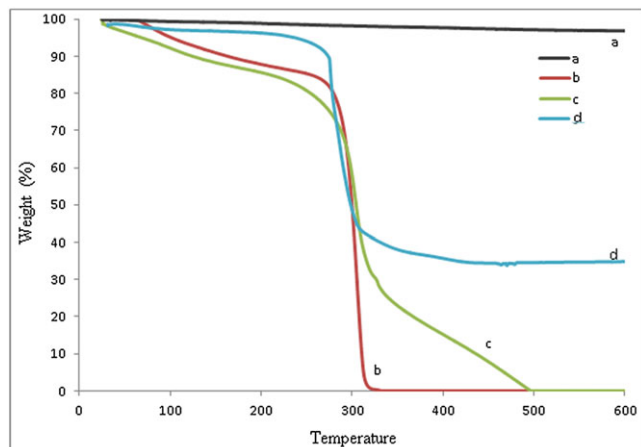


FIGURE 9 TGA curves for the synthesized (a) nano-Fe₃O₄, (b) cellulose, (c) Cellulose-NH₂ and (d) nano-Fe₃O₄@Cellulose-NH₂-CuI

decomposition of cellulose chains over Fe₃O₄ NPs and CuI. The remaining weight loss for nano-Fe₃O₄@Cellulose-NH₂-CuI at temperature higher than 300 °C is related to the Fe₃O₄ and CuI that are loaded in the composite.

3.3 | Computation

3.3.1 | Computational details

Recently, we have assessed computationally metal–ligand interactions in modified poly(styrene-*co*-maleic anhydride) palladium nanocatalyst,^[44] copper(I) aminated KIT-5^[38] and APTES-KIT-5 mesoporous silica-supported copper(II) acetate complex^[45] via quantum chemistry approaches. Armed with these experiences, we present a quantitative description for metal–ligand interactions in the nano-Fe₃O₄@Cellulose-NH₂-CuI complex by performing density functional theory (DFT)^[46] and quantum theory of atoms in molecules (QTAIM) computations.^[47,48] In this respect, we have designed an effective model for cellulose-NH₂ (ligand **1**) and nano-Fe₃O₄@Cellulose-NH₂-CuI (complex **2**) considering that this model is a credible comprise between accuracy and time-saving efficiency of computational procedure. We first determined the optimized structure of compounds **1** and **2** using the M06 method in combination with the basis sets 6-31G for C, H, O and N atoms and 6-31G(d) for Si atom, and in the cases of Cu, Fe and I atoms, the effective core potential, LANL2DZ, were used together with the accompanying basis set to describe the valence electron density.^[49] It should be mentioned that M06 functional has been introduced recently as a hybrid meta-GGA (generalized gradient approximation) exchange-correlation functional that was parameterized including both transition metals and non-metals and was recommended for application in organometallic and thermochemistry, kinetic studies and noncovalent interactions.^[50] The stationary points were determined as minima through verifying the presence of all real frequencies. All DFT computations were performed using the Gaussian 09 suite of programs.^[51]

3.3.2 | Computational assessment

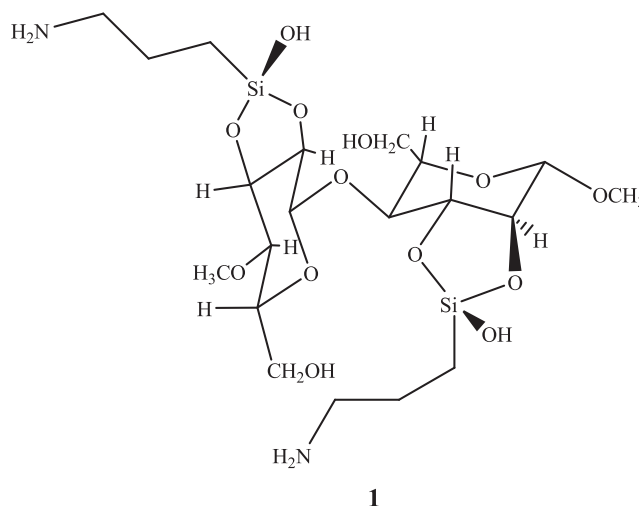
On the basis of our obtained DFT and QTAIM computational results, we can present a quantitative description for metal–ligand interactions of the nano-Fe₃O₄@Cellulose-NH₂-CuI complex **2**.

In this case, structures **1** and **2** are considered as simple models for cellulose-NH₂ ligand and nano-Fe₃O₄@Cellulose-NH₂-CuI complex, respectively (Scheme 2). Also, a tetrahedrally coordinated high-spin Fe(III) moiety has been considered as a model for nano-Fe₃O₄ with inverse spinel crystal lattice structure. The choice of the position of the tethered Si side chain on the ring is arbitrary, as upon surveying the pertinent literature it appeared that, because of the complex structure of the FT-IR spectrum, no attempt to precisely assign the newly formed Si–O bonds was made in any of the previous researches. Additionally, our calculation on another complex structure involving the exchanged positions of CuI and Fe moieties resulted in a complex which is 38.6 kcal mol^{−1} higher in energy than **2**, and as a consequence, further calculations were performed on **2** as found to be the more stable structure.

In Figure 10, we present the optimized geometries of ligand **1** and complex **2** calculated using the M06 method with the atomic numbering. In Figure 10, we also present M06 calculated C–N bond length (and also bond order in parentheses) in each of **1** and **2**. Comparative survey of the optimized structures of **1** and **2** demonstrates a geometrical deformation in **1** through complexation. In the following, the structural stability of **2** is analysed based on the various electronic indicators.

The bond orders of some key bonds in **1** with their corresponding bonds in complex **2** are listed in Table 1 to characterize the variation of bond orders via complexation. The data in Table 1 demonstrate that the bond order of C1–N1, C2–N2, C4–O2 and C3–O1 bonds decreases in **2** compared to **1**, through complexation.

In the next step, we focused on topological analysis of electron density via the QTAIM method^[48,49] to interpret



SCHEME 2 Simple model for cellulose-NH₂ ligand

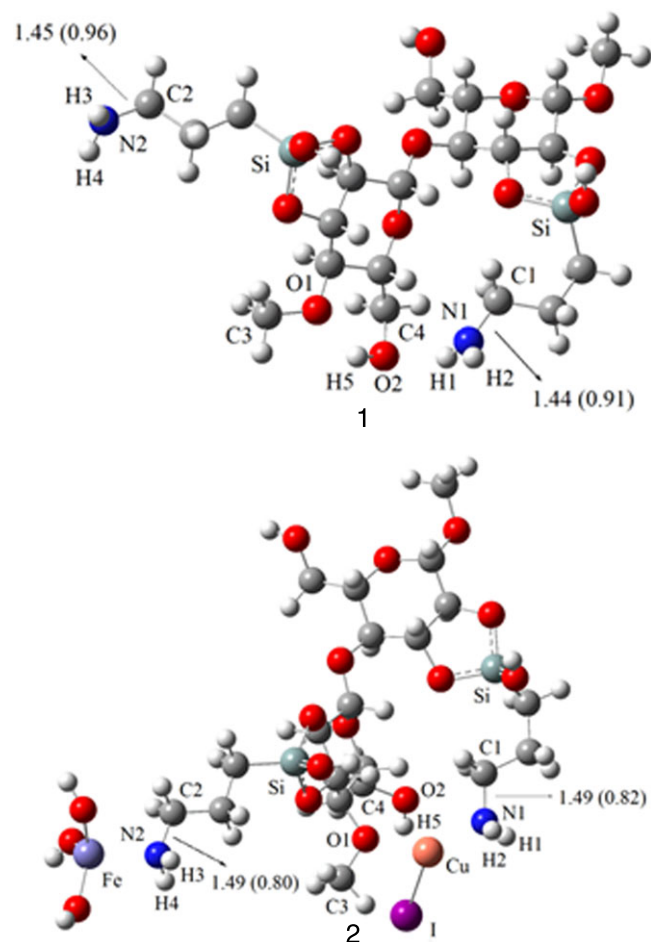


FIGURE 10 Atomic numbering and optimized structures obtained at M06/6-31G level of theory for **1** and **2**. Also shown are the C–N bond lengths (and bond orders) calculated at M06/6-31G level of theory

the nature of metal–ligand interactions in complex **2**. In this respect, we analysed M06/6-31G calculated wave function of electron density using the Multiwfn program package.^[52] QTAIM molecular graphs of ligand **1** and complex **2** including all bond and ring critical points and their associated bond paths are displayed in Figure 11.

Table 2 gives the QTAIM calculated values of electron density, ρ_b , its Laplacian, $\nabla^2\rho_b$, electronic kinetic energy density, G_b , electronic potential energy density, V_b , total electronic energy density, H_b , and $|V_b|/G_b$ ratio at some selected bond critical points (BCPs) for ligand **1** and complex **2**. It is important to mention that the electron density at BCPs usually corresponds to the strength of the bond between two atoms. Values of $\rho_b < 0.1$ au are indicative of an electrostatic interaction; it is usually correlated with a relatively small and positive value of $\nabla^2\rho_b$.^[49–52] By contrast, for a covalent interaction, usually $\rho_b > 0.1$ au and $\nabla^2\rho_b$ is usually negative with the same order as ρ_b .^[48–52] Moreover, a good authentic indicator for classifying interatomic interactions is the total electronic energy density that is defined as $H_b = G_b + V_b$ at BCPs. For electrostatic interactions, H_b has a positive value and for covalent interactions it is negative.

TABLE 1 Calculated values of some selected bond orders in ligand **1** and complex **2** obtained at M06/6-31G level of theory (numbering of atoms is in accordance with Figure 10)

Bonded atoms	Ligand 1	Complex 2
N1–C1	0.913	0.820
N1–H1	0.796	0.803
N1–H2	0.863	0.815
O2–H5	0.721	0.717
O2–C4	0.875	0.833
O1–C3	0.786	0.741
N2–C2	0.957	0.796
N2–H3	0.858	0.809
N2–H4	0.859	0.809
N1–Cu	—	0.380
O1–Cu	—	0.205
O2–Cu	—	0.199
Cu–I	—	0.946
N2–Fe	—	0.281
H5–I	—	0.076

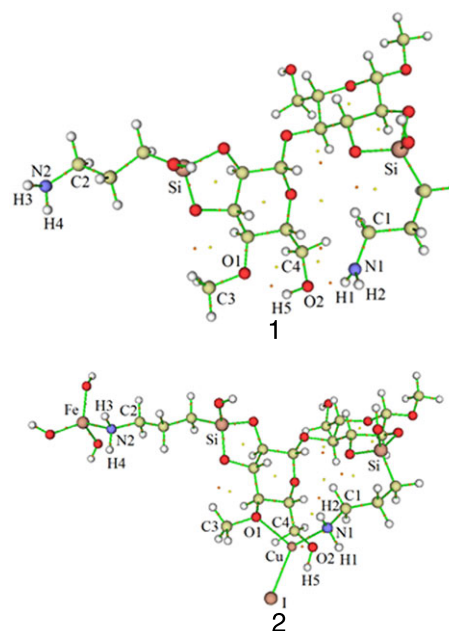


FIGURE 11 Complete molecular graphs of **1** and **2** obtained using QTAIM analysis of M06/6-31G electron density functions. BCPs: brown circles; ring critical points: yellow circles; bond paths: green lines

On the basis of the results collected in Table 2, the following can be stated: (i) through complexation, calculated values of ρ_b decrease at N1–C1, N2–C2, O2–C4 and O1–C3 BCPs, which confirms the donation of shared electrons to the metal centres; (ii) the large values of electron density together with the negative values of $\nabla^2\rho_b$ and H_b at N1–C1, N2–C2, O2–C4, O1–C3 and N–Hs BCPs indicate the covalent character of these chemical bonds in **1** and **2**; and (iii) the small values of electron density with the positive values of $\nabla^2\rho_b$ and H_b at N1–Cu, O1–Cu, O2–Cu and N2–Fe BCPs demonstrate that the

TABLE 2 Mathematical properties of some selected BCPs in ligand **1** and complex **2**. The properties have been obtained via QTAIM analysis of the M06/6-31G calculated wave function of electron density (numbering of atoms is in accordance with Figure 10)

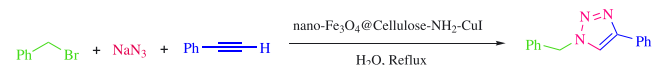
Bonded atoms of BCPs	ρ_b	$\nabla^2\rho_b$	G_b	V_b	H_b	$ V_b /G_b$
Ligand 1						
N1—C1	0.2545	−0.5803	0.1189	−0.3829	−0.2640	3.2204
N2—C2	0.2515	−0.5618	0.1167	−0.3738	−0.2571	3.2031
O1—C3	0.2178	−0.2637	0.1698	−0.4055	−0.2357	2.3883
O2—H5	0.3226	−0.1523	0.0631	−0.5070	−0.4439	8.0386
O2—C4	0.2312	−0.3688	0.1544	−0.4010	−0.2466	2.5972
Complex 2						
N1—C1	0.2301	−0.4438	0.1073	−0.3255	−0.2182	3.0336
N2—C2	0.2288	−0.4393	0.1127	−0.3353	0.2226	2.9752
O1—C3	0.2104	−0.2165	0.1709	−0.3959	−0.2250	2.3166
O2—H5	0.3203	−0.1513	0.6190	−0.5020	−0.4401	0.8110
O2—C4	0.2232	−0.3214	0.1546	−0.3895	−0.2349	2.5194
N1—Cu	0.0745	0.4756	0.1194	−0.1198	−0.0005	1.0034
O1—Cu	0.0386	0.2334	0.0526	−0.0468	0.0058	0.8902
O2—Cu	0.0307	0.1240	0.0313	−0.0315	−0.0003	1.0004
Cu—I	0.0519	0.1368	0.417	−0.0492	−0.0075	1.1795
N2—Fe	0.0678	0.3559	0.0921	−0.0953	−0.0031	1.0341

metal–ligand interactions do not have covalent character. For N1—Cu, O1—Cu and O2—Cu BCPs, calculated values of $1 < |V_b|/G_b < 2$ confirm the presence of partially covalent–electrostatic interactions.

3.4 | Application of Nano-Fe₃O₄@Cellulose-NH₂-CuI magnetic catalyst

After the successful preparation and characterization of the nano-Fe₃O₄@Cellulose-NH₂-CuI magnetic catalyst, its catalytic activity with different weight ratios of CuI was examined using a model reaction of benzyl bromide, phenylacetylene and sodium azide (Huisgen cycloaddition reaction), to obtain 1-benzyl-4-phenyl-1*H*-1,2,3-triazole (**4a**) (Scheme 3), as sole product, using 0.01 g of magnetic composite under reflux in water. The products are obtained in high yield and excellent regioselectivity. The result shows that this click reaction proceeds with regioselectivity, among other merits, resulting from the use of this novel catalyst system for the aforementioned model reaction. In order to establish the strategy, various terminal alkynes, substituted benzyl bromides and sodium azide were reacted in the presence of catalytic amounts of nano-Fe₃O₄@Cellulose-NH₂-CuI to afford the corresponding 1,4-disubstituted 1,2,3-triazoles, regioselectively and in good yields.

As evident from Table 3, the catalytic performance of magnetic composite with a weight ratio of 2:1:1 of Cellulose-NH₂:nano-Fe₃O₄:CuI gives the best result (Table 3, entry 5). It is observed that increasing the CuI loading in the magnetic composite does not result in any improvement in the yields.

**SCHEME 3** Click reaction catalysed by nano-Fe₃O₄@Cellulose-NH₂-CuI

Therefore, the weight ratio of Cellulose-NH₂:nano-Fe₃O₄:CuI of 2:1:1 was selected. The copper loading in nano-Fe₃O₄@Cellulose-NH₂-CuI was determined using atomic absorption spectroscopy. For this purpose, the magnetic composite was dissolved in aqua regia (3:1 HCl–HNO₃) solution, filtered and analysed. Cu loading in nano-Fe₃O₄@Cellulose-NH₂-CuI was found to be 2 wt%. Comparison of EDX (Figure 3) and atomic absorption analysis of nano-Fe₃O₄@Cellulose-NH₂-CuI confirms the loading of copper to the modified support, which is a good evidence for the formation of metal complex with anchored ligand.

The reaction of benzyl bromide, sodium azide and phenylacetylene was selected as a model reaction in various solvents, temperatures and loadings of magnetic catalyst. The results for the optimization of the reaction conditions are summarized in Table 4. The reaction proceeds in refluxing water, giving the highest yield of product for which an inert atmosphere is not required (Table 4, entry 4). We carried out the model reaction in the presence of nano-Fe₃O₄@Cellulose-NH₂ as a catalyst under reflux in water and a poor yield of product is obtained even after 2 h (Table 4, entries 9 and 10). As expected, the reaction does not proceed in the absence of the catalyst, even after prolonged reaction time (Table 4, entry 8). This indicates that

TABLE 3 Optimization of CuI for magnetic catalyst in model reaction

Entry	Cellulose-NH ₂ (g)	Nano-Fe ₃ O ₄ :CuI (g)	Yield (%)
1	1	0.5:0.1	37
2	1	0.5:0.2	50
3	1	0.5:0.3	70
4	1	0.5:0.4	85
5	1	0.5:0.5	95
6	1	0.05:0.6	95

TABLE 4 Optimization of three-component synthesis of 1-benzyl-4-phenyl-1*H*-1,2,3-triazole (**4a**)^a

Entry	Catalyst (g)	Conditions	Time (h:min)	Yield (%) ^b
1	Nano-Fe ₃ O ₄ @Cellulose-NH ₂ -CuI (0.01)	H ₂ O/r.t.	2:00	Trace
2	Nano-Fe ₃ O ₄ @Cellulose-NH ₂ -CuI (0.01)	H ₂ O/50 °C	0:20	35
3	Nano-Fe ₃ O ₄ @Cellulose-NH ₂ -CuI (0.01)	H ₂ O/75 °C	0:20	82
4	Nano-Fe ₃ O ₄ @Cellulose-NH ₂ -CuI (0.01)	H ₂ O/reflux	0:20	95
5	Nano-Fe ₃ O ₄ @Cellulose-NH ₂ -CuI (0.01)	H ₂ O/110 °C	0:20	95
6	Nano-Fe ₃ O ₄ @Cellulose-NH ₂ -CuI (0.015)	H ₂ O/reflux	0:20	95
7	Nano-Fe ₃ O ₄ @Cellulose-NH ₂ -CuI (0.005)	H ₂ O/reflux	0:20	53
8	—	H ₂ O/reflux	12:00	—
9	Nano-Fe ₃ O ₄ @Cellulose-NH ₂ (0.01)	H ₂ O/reflux	2:00	Trace
10	Nano-Fe ₃ O ₄ @Cellulose-NH ₂ (0.02)	H ₂ O/reflux	2:00	Trace
11	Nano-Fe ₃ O ₄ @Cellulose-NH ₂ -CuI (0.01)	Solvent free/100 °C	2:00	62
12	Nano-Fe ₃ O ₄ @Cellulose-NH ₂ -CuI (0.01)	DMF/100 °C	2:00	45
13 ^c	Nano-Fe ₃ O ₄ @Cellulose-NH ₂ -CuI (0.01)	Toluene/100 °C	2:00	56
14 ^c	Nano-Fe ₃ O ₄ @Cellulose-NH ₂ -CuI (0.01)	Ethanol/reflux	0:20	85
15 ^c	Nano-Fe ₃ O ₄ @Cellulose-NH ₂ -CuI (0.01)	H ₂ O–DMSO (2:1)/reflux	2:00	50
16 ^c	Nano-Fe ₃ O ₄ @Cellulose-NH ₂ -CuI (0.01)	CH ₃ CN/reflux	2:00	70

^aReaction conditions: benzyl bromide (1 mmol), sodium azide (1.1 mmol), phenylacetylene (1 mmol) and catalyst (0.010 g) in water under reflux.

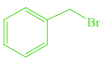
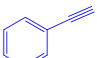
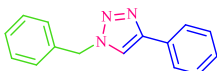
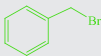
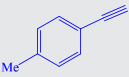
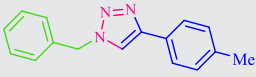
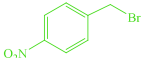
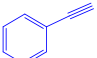
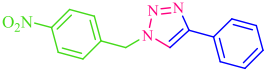
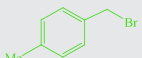
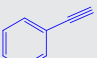
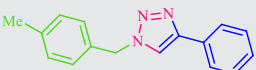
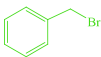

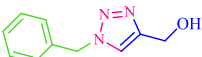
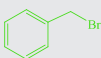

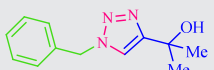
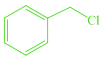
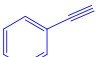
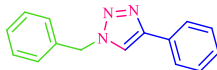
^bIsolated yield.

^cSolvent (2 ml).

nano-Fe₃O₄@Cellulose-NH₂-CuI as a catalyst plays a crucial role in the synthesis of **4a**. A higher reaction temperature or catalyst amount does not make an obvious difference in the yield of product (Table 4, entries 5, 6). But, a lower amount of catalyst decreases the yield of the reaction (Table 4, entry 7). Accordingly, the best results are obtained when the reaction is performed under reflux in water in the presence of 0.01 g of nano-Fe₃O₄@Cellulose-NH₂-CuI.

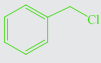
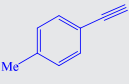
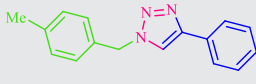
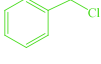
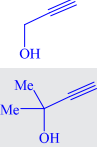
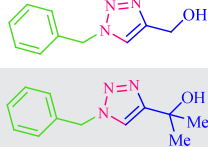
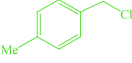
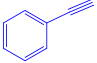
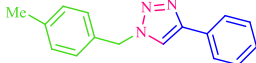
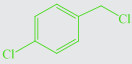
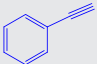
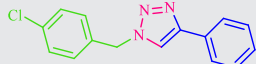
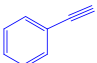
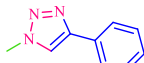
Thus, with the optimized reaction conditions in hand, the substrate scope of reaction was extended to various structurally diverse terminal alkynes and benzyl halides (Table 5). In general, various substituted phenylacetylenes and benzyl halides bearing electron-donating substituents as well as electron-withdrawing groups provide an array of 1,4-disubstituted 1,2,3- triazoles smoothly and cleanly, in good to excellent yields (75–95%) within relatively short times

TABLE 5 Three-component click reaction of benzyl halides, terminal alkynes and sodium azide using nano-Fe₃O₄@Cellulose-NH₂-CuI magnetic catalyst^a

Entry	Halide precursor	Alkyne	Product	Time (min)	Yield (%) ^b
1				20	95
2				25	88
3				30	85
4				20	88
5				25	90
6				30	89
7				25	90
8				25	83

(Continues)

TABLE 5 (Continued)

Entry	Halide precursor	Alkyne	Product	Time (min)	Yield (%) ^b
9				20	87
10				25	87
11				30	85
12				25	86
13	CH ₃ I			180	66

^aReaction conditions: alkyl halide (1 mmol), sodium azide (1.1 mmol), acetylene (1 mmol) and nano-Fe₃O₄@Cellulose-NH₂-CuI (0.010 g), H₂O (2 ml), reflux.

^bIsolated yield.

(15–80 min). As shown in Table 5, the aliphatic terminal alkynes bearing hydroxyl as functional group gave the desired triazoles in high yields.

3.5 | Recycling and leaching of catalyst

One of the main advantages of magnetic catalysts is their ease of separation as well as their reusability in further runs.^[53] In this regard, the recyclability of the nano-Fe₃O₄@Cellulose-NH₂-CuI magnetic catalyst was practically examined in a one-pot synthesis of **4a** under optimized conditions. A model reaction was conducted four times with recycled catalyst under similar conditions and no appreciable loss of weight was observed in the obtained desired compound. After each cycle, the catalyst was removed using a magnet, washed with water and ethyl acetate, dried in an oven at 70 °C and reused in another run of the model reaction without any further modification. This process was carried out over four runs and all reactions

led to desired products without significant changes in terms of the reaction time and yield. The yields for the four runs were found to be 95, 92, 90 and 89%, respectively (Figure 12). In addition only negligible difference between the copper content of fresh and the reused catalyst was observed as determined using atomic absorption spectroscopy, indicating the low amount of CuI catalyst leaching into the reaction mixture.

4 | CONCLUSIONS

In this study we have used magnetic modified cellulose as an inexpensive and biodegradable support for stabilization of CuI. The novel composite demonstrated efficient catalytic activity in terms of yield and reaction time in outstanding synthesis of 1,4-disubstituted 1,2,3-triazoles. Short reaction time, high yield, recyclability and reusability of the catalyst are the main notable advantages of this methodology which make the protocol economic.

ACKNOWLEDGMENTS

FN is gratefully acknowledge the financial support from Semnan University Research Council. MMH is thankful to Iran National Science Foundation (INSF) for its financial support and Alzahra University research council for the encouragements.

REFERENCES

- [1] S. Eyley, W. Thielemans, *Nanoscale* **2014**, *6*, 7764.
- [2] S. Ummartyotin, H. Manuspiya, *Renew. Sustain. Energy Rev.* **2015**, *41*, 402.
- [3] A. Mohammadinezhad, M. A. Nasseri, M. Salimi, *RSC Adv.* **2014**, *4*, 39870.

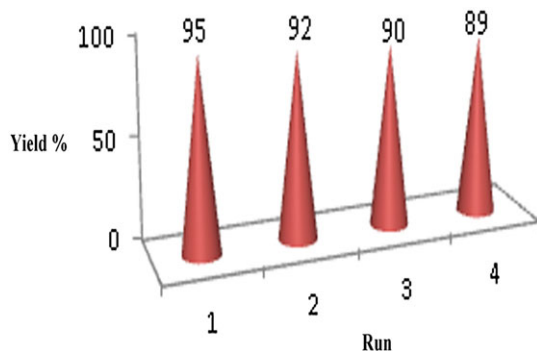


FIGURE 12 Recycling results for nano-Fe₃O₄@Cellulose-NH₂-CuI magnetic catalyst

- [4] N. Lavoine, I. Desloges, A. Dufresne, J. Bras, *Carbohydr. Polym.* **2012**, *90*, 735.
- [5] Y. Habibi, *Chem. Soc. Rev.* **2014**, *43*, 1519.
- [6] P. Chauhan, N. Yan, *RSC Adv.* **2015**, *5*, 37517.
- [7] Q. Yang, X. Pan, *J. Appl. Polym. Sci.* **2010**, *117*, 3639.
- [8] W. Zhang, B. Liu, B. Zhang, G. Bian, Y. Qi, X. Yang, C. Li, *Angew. Chem. Int. Ed.* **2015**, *466*, 210.
- [9] R. B. N. Baig, R. S. Varma, *Chem. Commun.* **2013a**, *49*, 752.
- [10] M. Jose Climent, A. Corma, S. Iborra, *RSC Adv.* **2012**, *2*, 16.
- [11] a) M. Kaushik, A. Moores, *Green Chem.* **2016**, *18*, 622; b) J. Safari, S. H. Banitaba, S. D. Khalili, *J. Mol. Catal. A* **2011**, *335*, 46.
- [12] a) M. G. Dekamin, M. Azimoshan, L. Ramezani, *Green Chem.* **2013**, *15*, 811; b) M. N. V. R. Kumar, *React. Funct. Polym.* **2000**, *46*, 1.
- [13] S. Wu, H. Ma, X. Jia, Y. Zhong, Z. Lei, *Tetrahedron* **2011**, *67*, 250.
- [14] S.-L. Cao, H. Xu, X.-H. Li, W.-Y. Lou, M.-H. Zong, *ACS Sustain. Chem. Eng.* **2015**, *3*, 1589.
- [15] T. Cheng, D. Zhang, H. Li, G. Liu, *Green Chem.* **2014**, *16*, 3401.
- [16] R. Hudson, *RSC Adv.* **2016**, *6*, 4262.
- [17] L. Casas, A. Roig, E. Rodríguez, E. Molins, J. Tejada, J. Sort, *J. Non-Cryst. Solids* **2001**, *285*, 37.
- [18] E. Ruijter, R. Scheffelaar, R. V. A. Orru, *Angew. Chem. Int. Ed.* **2011**, *50*, 6234.
- [19] G. Mohammadi Ziarani, Z. Hassanzadeh, P. Gholamzadeh, S. Asadi, A. Badii, *RSC Adv.* **2016**, *6*, 21979.
- [20] H. C. Kolb, M. G. Finn, K. B. Sharpless, *Angew. Chem. Int. Ed.* **2001**, *40*, 2004.
- [21] a) P. Thirumurugan, D. Matosiuk, K. Jozwiak, *Chem. Rev.* **2013**, *113*, 4905; b) W. Xi, T. F. Scott, C. J. Kloxin, C. N. Bowman, *Adv. Funct. Mater.* **2014**, *24*, 2572; c) R. Pola, A. Braunova, R. Laga, M. Pechar, K. Ulbrich, *Polym. Chem.* **2014**, *5*, 1340.
- [22] M. Whiting, J. Muldoon, Y.-C. Lin, S. M. Silverman, W. Lindstrom, A. J. Olson, H. C. Kolb, M. G. Finn, K. B. Sharpless, J. H. Elder, V. V. Fokin, *Angew. Chem. Int. Ed.* **2006**, *45*, 1435.
- [23] H. Gallardo, G. Conte, F. Bryk, M. C. S. Lourenço, M. S. Costa, V. F. Ferreira, *J. Braz. Chem. Soc.* **2007**, *18*, 1285.
- [24] D. R. Buckle, C. J. M. Rockell, H. Smith, B. A. Spicer, *J. Med. Chem.* **1986**, *29*, 2262.
- [25] a) M. K. Singh, R. Tilak, G. Nath, S. K. Awasthi, A. Agarwal, *Eur. J. Med. Chem.* **2013**, *63*, 635; b) Z. Ke, H.-F. Chow, M.-C. Chan, Z. Liu, K.-H. Sze, *Org. Lett.* **2012**, *14*, 394; c) Y. Hua, A. H. Flood, *Chem. Soc. Rev.* **2010**, *39*, 1262.
- [26] F. Alonso, Y. Moglie, G. Radivoy, *Acc. Chem. Res.* **2015**, *48*, 2516.
- [27] a) M. Meldal, C. W. Tornøe, *Chem. Rev.* **2008**, *108*, 2952; b) C. O. Kappe, E. Van der Eycken, *Chem. Soc. Rev.* **2010**, *39*, 1280; c) V. D. Bock, H. Hiemstra, J. H. van Maarseveen, *Eur. J. Org. Chem.* **2006**, *51*; d) J. S. Yadav, B. V. S. Reddy, G. M. Reddy, D. N. Chary, *Tetrahedron Lett.* **2007**, *48*, 8773.
- [28] a) B. Dervaux, F. E. D. Prez, *Chem. Sci.* **2012**, *3*, 959; b) T. Jin, M. Yan, Y. Yamamoto, *ChemCatChem* **2012**, *4*, 1217.
- [29] N. Madhavan, C. W. Jones, M. Weck, *Acc. Chem. Res.* **2008**, *41*, 1153.
- [30] S. Chassaing, A. Alix, T. Boningari, K. Sani Souna Sido, M. Keller, P. Kuhn, B. Louis, J. Sommer, P. Pale, *Synthesis* **2010**, 1557.
- [31] I. Jlalía, H. Elamari, F. Meganem, J. Herscovici, C. Girard, *Tetrahedron Lett.* **2008**, *49*, 6756.
- [32] U. Sirion, Y. J. Bae, B. S. Lee, D. Y. Chi, *Synlett* **2008**, 2326.
- [33] M. Chichigrovsky, A. Primo, P. Gonzalez, K. Molvinger, M. Robitzer, F. Quignard, F. Taran, *Angew. Chem.* **2009**, *121*, 6030.
- [34] R. Mirsafaei, M. M. Heravi, S. Ahmadi, M. H. Moslemin, T. Hosseinejad, *J. Mol. Catal. A* **2015**, *402*, 100.
- [35] R. B. N. Baig, R. S. Varma, *Green Chem.* **2013b**, *15*, 1839.
- [36] a) F. Nemati, M. M. Heravi, R. Saeedi Rad, *Chin. J. Catal.* **2012**, *33*, 1825; b) F. Janati, M. M. Heravi, A. M. Shokraie, *Synth. React. Inorg. Met. Org. Chem.* **2015**, *45*, 1.
- [37] a) F. Nemati, M. M. Heravi, A. Elhampour, *RSC Adv.* **2015**, *5*, 45775; b) A. Elhampour, F. Nemati, M. Kaveh, *Chem. Lett.* **2016**, *45*, 226; c) F. Nemati, A. Elhampour, H. Farrokhi, M. Bagheri Natanzi, *Catal. Commun.* **2015**, *66*, 15; d) F. Nemati, A. Elhampour, M. B. Natanzi, S. Sabaqian, *J. Iran. Chem. Soc.* **2016**, *13*, 1045; e) F. Nemati, A. Elhampour, S. Zulfaghari, Phosphorus, *Sulfur Silicon Relat. Elem.* **2015**, *190*, 1692; f) M. M. Heravi, Z. Faghihi, *J. Iran. Chem. Soc.* **2014**, *11*, 209; g) M. M. Heravi, E. Hashemi, Y. S. Beheshtiha, K. Kamjou, M. Toolabi, N. Hosseintash, *J. Mol. Catal. A* **2014**, *392*, 173; h) M. M. Heravi, F. Mousavizadeh, N. Ghobadi, M. Tajbakhsh, *Tetrahedron Lett.* **2014**, *55*, 1226.
- [38] a) M. M. Heravi, A. Fazeli, H. A. Oskooie, Y. S. Beheshtiha, H. Valizadeh, *Synlett* **2012**, *23*, 2927; b) E. Hashemi, Y. S. Beheshtiha, S. Ahmadi, M. M. Heravi, *Transition Met. Chem.* **2014**, *39*, 593; c) M. M. Heravi, H. Hamidi, V. Zadsirjan, *Curr. Org. Synth.* **2014**, *11*, 647; d) R. Mirsafaei, M. M. Heravi, S. Ahmadi, M. S. Moslemin, T. Hosseinejad, *J. Mol. Catal. A* **2015**, *402*, 100.
- [39] X. Sun, L. Yang, Q. Li, J. Zhao, X. Li, X. Wang, H. Liu, *Chem. Eng. J.* **2014**, *241*, 175.
- [40] A. Sarkar, S. K. Biswas, P. Pramanik, *J. Mater. Chem.* **2010**, *20*, 4417.
- [41] Z. Souguir, A.-L. Dupont, K. Fatyeyeva, G. Mortha, H. Cheradame, S. Ipert, B. Lavedrine, *RSC Adv.* **2012**, *2*, 7470.
- [42] L. Li, Y. Dou, L. Wang, M. Luo, J. Liang, *RSC Adv.* **2014**, *4*, 25658.
- [43] M. M. Heravi, E. Hashemi, Y. S. Beheshtiha, S. Ahmadi, T. Hosseinejad, *J. Mol. Catal. A* **2014**, *394*, 74.
- [44] R. Mirsafaei, M. M. Heravi, T. Hosseinejad, S. Ahmadi, *Appl. Organomet. Chem.* **2016**, *30*, 823.
- [45] C. Lee, W. Yang, R. G. Parr, *Phys. Rev. B* **1988**, *37*, 785.
- [46] R. F. W. Bader, *Atoms in Molecules: A Quantum Theory*, Oxford University Press, Oxford **1990**.
- [47] R. G. A. Bone, R. F. W. Bader, *J. Chem. Phys.* **1996**, *100*, 10892.
- [48] V. A. Nasluzov, G. L. Gutsev, V. K. Gryaznov, *J. Struct. Chem.* **1990**, *31*, 851.
- [49] Y. Zhao, D. G. Truhlar, *Theor. Chem. Acc.* **2008**, *120*, 215.
- [50] M. J. Frisch, G. W. Trucks, H. B. Schlegel, G. E. Scuseria, M. A. Robb, J. R. Cheeseman, G. Scalmani, V. Barone, B. Mennucci, G. A. Petersson, H. Nakatsuji, M. Caricato, X. Li, H. P. Hratchian, A. F. Izmaylov, J. Bloino, G. Zheng, J. L. Sonnenberg, M. Hada, M. Ehara, K. Toyota, R. Fukuda, J. Hasegawa, M. Ishida, T. Nakajima, Y. Honda, O. Kitao, H. Nakai, T. Vreven, J. A. Montgomery Jr., J. E. Peralta, F. Ogliaro, M. Bearpark, J. J. Heyd, E. Brothers, K. N. Kudin, V. N. Staroverov, R. Kobayashi, J. Normand, K. Raghavachari, A. Rendell, J. C. Burant, S. S. Iyengar, J. Tomasi, M. Cossi, N. Rega, J. M. Millam, M. Klene, J. E. Knox, J. B. Cross, V. Bakken, C. Adamo, J. Jaramillo, R. Gomperts, R. E. Stratmann, O. Yazyev, A. J. Austin, R. Cammi, C. Pomelli, J. W. Ochterski, R. L. Martin, K. Morokuma, V. G. Zakrzewski, G. A. Voth, P. Salvador, J. J. Dannenberg, S. Dapprich, A. D. Daniels, O. Farkas, J. B. Foresman, J. V. Ortiz, J. Cioslowski, D. J. Fox, *Gaussian 09, Revision A.1*, Gaussian Inc., Wallingford, CT **2009**.
- [51] T. Lu, F. Chen, *J. Comput. Chem.* **2014**, *33*, 580.
- [52] R. F. W. Bader, H. Essén, *J. Chem. Phys.* **1984**, *80*, 1943.
- [53] X. Zhang, P. Li, Y. Ji, L. Zhang, L. Wang, *Synthesis* **2011**, 2975.

How to cite this article: Sabaqian, S., Nemati, F., Heravi, M. M., and Nahzomi, H. T. (2016), Copper (I) iodide supported on modified cellulose-based nano-magnetite composite as a biodegradable catalyst for the synthesis of 1,2,3-triazoles, *Appl Organometal Chem*, doi: 10.1002/aoc.3660